PDE-Based Color Morphology Using Matrix Fields

Ali Sharifi Boroujerdi[1(✉)], Michael Breuß[1], Bernhard Burgeth[2], and Andreas Kleefeld[1]

[1] Faculty of Mathematics, Natural Sciences and Computer Science, Brandenburg Technical University Cottbus-Senftenberg, 03046 Cottbus, Germany
{boroujerdi,breuss,kleefeld}@tu-cottbus.de
[2] Department of Mathematics and Computer Science, Saarland University, 66123 Saarbrücken, Germany
burgeth@math.uni-sb.de

Abstract. In this work, we propose a novel way for performing operations of mathematical morphology on color images. To this end, we convert pixelwise the *rgb*-values into symmetric 2×2 matrices. The new color space can be interpreted geometrically as a biconal color space structure. Motivated by the formulation of the fundamental morphological operations dilation and erosion in terms of partial differential equations (PDEs), we show how to define finite difference schemes making use of the matrix field formulation. The computation of a pseudo supremum and a pseudo infimum of three color matrices is a crucial step for setting up advanced PDE-based methods. We show that this can be achieved for our goal by an algebraic technique. We investigate our approach by dedicated experiments and confirm useful properties of the new PDE-based color morphology operations.

Keywords: PDE-based morphology · Matrix fields · Color morphology · Finite difference schemes · FCT scheme · Pseudo supremum · Pseudo infimum

1 Introduction

In modern digital imagery color images are very common, as e.g. smartphones often feature a digital camera yielding color images. With abundant sources of available color information, it becomes increasingly important to consider this information in the construction of image processing tools.

A fundamental class of image analysis processes are the methods of mathematical morphology pioneered by Serra and Matheron [16,22]. Morphological processing is a nonlinear method consisting of operations on sets of pixels arranged in structuring elements. The building blocks of mathematical morphology for gray-scale images are the processes of *dilation* and *erosion*. Many other processes such as opening, closing, top hats, and other morphological operators such as derivatives can be derived from these two operations.

J.-F. Aujol et al. (Eds.): SSVM 2015, LNCS 9087, pp. 461–473, 2015.
DOI: 10.1007/978-3-319-18461-6_37

Considering the important underlying mathematical structure of these operations, it is required that one can define a total order of the values contributing in a structuring element. While for gray-scale images the corresponding lattice theory framework is satisfactory and adequate, the extension of this concept to work with colors is difficult because of the lack of a total order for vector-valued data such as *rgb* values. Therefore, performing even the simplest morphological operation on color images is not trivial.

There have been numerous attempts to establish a morphological framework for color images. Generally speaking, the use of ranking schemes and properly defined extremal operators as substitutes for maxima and minima are the main building blocks in these attempts, see e.g. [3,12,13,23]. For a conceptually different development, let us mention here the approach by Van de Gronde *et al.* [14] that relies on a partial order rather than a total order. However, one may conclude that the optimal way to define morphological operations on color images is still an open issue and that a proper solution might depend on the purpose of the filtering.

In this paper, we tackle the issue from a different point of view. To this end, we combine two existing approaches to mathematical morphology in order to formulate our novel strategy for color image morphology.

The first approach we consider is the formulation of dilation and erosion in terms of partial differential equations (PDEs), see [2,4,6,19,21]. Mimicking a special wave propagation process, the arising PDEs are hyperbolic Hamilton-Jacobi equations. Then, important numerical methods for discretizing the PDEs for dilation and erosion in the gray-value setting are the schemes of Rouy and Tourin [19], Osher and Sethian [18] and the flux-corrected transport (FCT) scheme of Breuß and Weickert [5]. Motivated by these developments and driven by an interest to filter data arising in diffusion tensor magnetic resonance imaging (DT-MRI), the PDE-based approach as well as the above mentioned schemes have been generalised to deal with specific matrix fields, see e.g. [7,8] and the references therein. The matrices defining the data for these PDE-based morphological methods are symmetric, positive semi-definite and of size three times three.

Secondly, we consider the developments in the recent work [11]. There, color images are embedded into matrix fields consisting of symmetric 2×2 matrices. For these, matrix-based operations are described that mimic dilation and erosion in the spirit of the classical, set-theoretic approach.

As indicated we combine in this work the above mentioned developments in defining PDE-based methods for mathematical morphology of color images. We employ the framework presented in [11] to transform *rgb* data into a bicone-shaped color space that corresponds to symmetric 2×2 matrices. For such matrices we define finite difference schemes that describe in the discrete sense the PDEs of morphological dilation/erosion.

While on the technical side this translation of the schemes as described e.g. in [7] to the color matrix framework seems at a first glance to be relatively straightforward, let us comment on several issues. First, let us note that the matrices we deal with here are not positive semidefinite. Thus, taking over technical parts from methods developed in the aforementioned DT-MRI context may not lead

to useful results. Secondly, and as a technical difference to the proceeding in [11], we do not employ here the procedures of addition and subtraction motivated by Einstein addition in Hilbert spaces. Furthermore, and again in the light of the many attempts in previous literature [3,12,13,23], let us stress that it is not at all self-evident that one obtains reasonable numerical results when constructing a method for the purpose of color morphology. However, for our approach we confirm experimentally that it does not give so-called false colors, cf. [23]. This means, that our PDE-based dilation and erosion processes may only lead to color modifications in the sense that they appear in higher and lower saturated versions of contributing colors, and not as a completely different color.

Paper Organisation. In accordance to the described paper contents, in Section 2 some background on the basic morphological operators is presented. In Section 3, the PDE concept behind our approach is introduced. Section 4 is devoted to recalling the transfer of *rgb* images to matrix fields. In Section 5, the solution of finding pseudo suprema and infima of three matrices is discussed which we need to define numerical schemes. Section 6 contains experimental results. We conclude the paper with some remarks in Section 7.

2 Morphological Operations and PDEs

Morphological Operations. We first give a brief account of the two operations that are at the basis of our developments, namely morphological dilation and erosion. As we seek to emphasize the underlying ideas here, we stick to a simple presentation.

A structuring element E is a mask that allows us to specify neighborhood structures in an image. Then one may use SEs to define morphological operators acting on them. For a given, initial image f we write the *dilation* and the *erosion* with such a structuring element E as

$$f \oplus E := \sup\{f(x-x', y-y') \,|\, (x', y') \in E\} \quad \text{and} \tag{1}$$

$$f \ominus E := \inf\{f(x-x', y-y') \,|\, (x', y') \in E\} \tag{2}$$

respectively. Making use of these building blocks, one can define e.g. morphological derivative operators. One which is useful in the context of this work is the so-called *morphological Laplacian* [23] which reads as

$$\Delta_E f \;:=\; (f \oplus E) - 2f + (f \ominus E) \tag{3}$$

As it is evident, the morphological Laplacian is a morphological counterpart of the second derivative of a function. It allows to distinguish regions influenced by brightness minima and maxima in an image. This is useful for defining so-called *shock filters*, see e.g. [17]. In the gray-value setting, one step of shock filtering applied pixelwise at an image f may be described as

$$S_E f \;:=\; \begin{cases} f \oplus E\,, & \Delta_E f < 0 \\ f\,, & \Delta_E f = 0 \\ f \ominus E\,, & \Delta_E f > 0 \end{cases} \tag{4}$$

As can be seen by considering (4), shock filtering amounts to applying dilation and erosion in order to enlarge brightness maxima and minima, respectively, while the transition line between these regions is managed by the morphological Laplacian. In a PDE-based setting as already described in [17], the dilation and erosion PDEs are solved iteratively in accordance to the process (4).

PDEs for Mathematical Morphology. Thinking of a gray-valued image as a discrete representation of a continuous-scale function, some of the geometric characteristics of continuous morphology are omitted in its discrete version. As an example, the definition of a disk-shaped structuring element is easy in the continuous plane but especially on a small scale this is difficult or even impossible to realize conveniently on a discrete grid.

To this end, it is necessary to specify continuous mathematical morphology from the angle of curve evolution. By this method, discrete mathematical morphology can be interpreted as the numerical implementation of a continuous-scale evolution.

According to [20] dilation can be performed at infinitesimal steps. This motion generates a set of velocity vectors, one for each point on the boundary of the disk-shaped (or more generally, convex) structuring element. For this purpose, let us parameterize these vectors by the angle θ running over all possible angles about a central point in the plane, so that $\theta \in [0, 2\pi]$. For a given initial image $f := f(x, y)$, where (x, y) denotes a point in the image domain Ω, let $u := u(x, y, t)$ be the image evolving under the process of interest in time t. Then we have

$$\partial_t u \;=\; \sup_{\theta} \{R(\theta) \cdot \nabla u\} \;, \tag{5}$$

where $R(\theta)$ is a function representing the boundary of the convex structuring element. In this way, the following velocities are obtained for popular structuring elements S:

$$\sup_{\theta} \{R(\theta) \cdot \nabla u\} \;=\; \begin{cases} \|\nabla u\|_1 \,, & S = \text{diamond} \\ \|\nabla u\|_2 \,, & S = \text{disk} \\ \|\nabla u\|_\infty \,, & S = \text{square} \end{cases} \tag{6}$$

Focusing again on the use of a disk-shaped structuring element and generalising the process to include erosion, we obtain the PDEs for gray-value dilation $(+)$ and erosion $(-)$ as

$$\partial_t u \;=\; \pm\|\nabla u\|_2 \;=\; \pm\sqrt{(\partial_x u)^2 + (\partial_y u)^2} \qquad \text{on} \qquad \Omega \times (0, \infty) \tag{7}$$

which we supplement by Neumann boundary conditions

$$\partial_n u = 0 \qquad \text{on} \qquad \partial\Omega \times (0, \infty) \tag{8}$$

and the initial condition defined by an input image f

$$u(x, y, 0) \;:=\; f(x, y) \qquad \forall (x, y) \in \Omega \tag{9}$$

While it is possible to describe already at this point a matrix-valued counterpart of the PDEs as in (7) as can be seen in [7,8], we refrain from this here for shortness of presentation.

3 Numerical Methods for the PDEs of Dilation and Erosion

In this part, we briefly survey the schemes mentioned in the introduction that we will also consider here for realizing our PDE-based approach. These are the first-order accurate *Rouy-Tourin (RT)* scheme which is proposed in [19], the second-order method of *Osher and Sethian (OS)* [18], and as a state-of-the-art approach we consider the *flux corrected transport (FCT)* algorithm [5].

Notice that we apply the symbol of $u^n_{i,j}$ as the gray-value of the evolving image u at the pixel located in the i^{th} row and j^{th} column of the image at the n^{th} time step during the morphological progress. We recall standard notations for backward and forward differences in x- and y-directions as follows:

$$\begin{aligned} D^x_- u^n_{i,j} &= u^n_{i,j} - u^n_{i-1,j}\,, \quad D^x_+ u^n_{i,j} = u^n_{i+1,j} - u^n_{i,j}\,, \\ D^y_- u^n_{i,j} &= u^n_{i,j} - u^n_{i,j-1}\,, \quad D^y_+ u^n_{i,j} = u^n_{i,j+1} - u^n_{i,j} \end{aligned} \tag{10}$$

Let us now consider a uniform pixel width h in both spatial grid directions in an image and a numerical time step size τ for the evolution. Our aim is now to discretise the PDE (7), sticking thereby for the presentation here to the case of *dilation* with a disk-shaped structuring element.

Then, in the *RT scheme*, the dilation operation is expressed by

$$u^{n+1}_{i,j} \;=\; u^n_{i,j} + \frac{\tau}{h}\sqrt{(\max(0, D^x_+ u^n_{i,j}, -D^x_- u^n_{i,j}))^2 + (\max(0, D^y_+ u^n_{i,j}, -D^y_- u^n_{i,j}))^2} \tag{11}$$

while the second-order *OS method* is given by

$$u^{n+1}_{i,j} \;=\; \frac{u^n_{i,j}}{2} + \frac{u^{-n+1}_{i,j}}{2} + \frac{\tau}{2h} L\left(u^{-n+1}, i, j\right)) \tag{12}$$

where

$$u^{-n+1}_{i,j} \;=\; u^n_{i,j} + \frac{\tau}{h} L\left(u^n, i, j\right)) \tag{13}$$

and

$$\begin{aligned} L(u^n, i, j) = \Bigg[& \left(\min\left\{ D^x_- u^n_{i,j} + \frac{1}{2}\mathrm{mm}(D^x_- D^x_+ u^n_{i,j}, D^x_- D^x_- u^n_{i,j}), 0 \right\} \right)^2 \\ & + \left(\max\left\{ D^x_+ u^n_{i,j} - \tfrac{1}{2}\mathrm{mm}(D^x_+ D^x_+ u^n_{i,j}, D^x_- D^x_+ u^n_{i,j}), 0 \right\} \right)^2 \\ & + \left(\min\left\{ D^y_- u^n_{i,j} + \tfrac{1}{2}\mathrm{mm}(D^y_- D^y_+ u^n_{i,j}, D^y_- D^y_- u^n_{i,j}), 0 \right\} \right)^2 \\ & + \left(\max\left\{ D^y_+ u^n_{i,j} - \tfrac{1}{2}\mathrm{mm}(D^y_+ D^y_+ u^n_{i,j}, D^y_- D^y_+ u^n_{i,j}), 0 \right\} \right)^2 \Bigg]^{\frac{1}{2}} \end{aligned} \tag{14}$$

The function $\mathrm{mm}(\cdot\,,\cdot)$ indicates the *minmod function* which is given as

$$\mathrm{mm}(\alpha, \beta) \;:=\; \begin{cases} \max(\alpha, \beta)\,, & \alpha < 0,\ \beta < 0 \\ \min(\alpha, \beta)\,, & \alpha > 0,\ \beta > 0 \\ 0\,, & \text{otherwise} \end{cases} \tag{15}$$

Let us also give a brief account of the *FCT scheme*. The main concept in the FCT scheme is to use the RT scheme in a *predictor step* in a first phase. Then the unwanted blurring effects generated by the first-order upwind derivatives in the RT scheme are measured to reverse the associated quantity in a *corrector step* that performs stabilized inverse diffusion.

Let us now write the values obtained after the predictor step performed by the RT scheme in the format $u^p_{i,j}$ at pixel (i,j). With the definitions

$$g_{i+1/2,j} := \mathrm{mm}\left(D^x_- u^p_{i,j},\, \frac{\tau}{2h} D^x_+ u^p_{i,j},\, D^x_+ u^p_{i+1,j}\right), \tag{16}$$

$$g_{i,j+1/2} := \mathrm{mm}\left(D^y_- u^p_{i,j},\, \frac{\tau}{2h} D^y_+ u^p_{i,j},\, D^y_+ u^p_{i,j+1}\right), \tag{17}$$

where $\mathrm{mm}(\cdot\,,\cdot\,,\cdot\,)$ is a straightforward extension of (15) and

$$Q_h := \sqrt{\left(\frac{\tau}{2h}\left|u^p_{i+1,j} - u^p_{i-1,j}\right|\right)^2 + \left(\frac{\tau}{2h}\left|u^p_{i,j+1} - u^p_{i,j-1}\right|\right)^2}, \tag{18}$$

$$Q_l := \sqrt{\left(\delta u^p_i\right)^2 + \left(\delta u^p_j\right)^2}, \tag{19}$$

where the stabilized inverse diffusive fluxes are given by

$$u^p_i := \frac{\tau}{2h}\left|u^p_{i+1,j} - u^p_{i-1,j}\right| + g_{i+1/2,j} - g_{i-1/2,j}\,, \tag{20}$$

$$u^p_j := \frac{\tau}{2h}\left|u^p_{i,j+1} - u^p_{i,j-1}\right| + g_{i,j+1/2} - g_{i,j-1/2}\,, \tag{21}$$

we can write the subsequent *corrector step* of the FCT scheme as

$$u^{n+1}_{i,j} \;=\; u^p_{i,j} + Q_h - Q_l \tag{22}$$

To summarise, a subsequent application of scheme (11) for obtaining predicted data $u^p_{i,j}$ – instead of $u^{n+1}_{i,j}$ in (11) – and the corrector step (22) making use of the predicted values is equivalent to the FCT scheme.

Finite Difference Methods for Dilation/Erosion of Color Data. Finally, our aim is to work with fields of symmetric 2×2 matrices which represent color data instead of gray-values. For the definition of corresponding numerical schemes, we proceed in a straightforward fashion building upon (10)–(22). Instead of the evolving gray-values $u^n_{i,j}$ we will plug in the 2×2 matrices $U^n_{i,j}$, with $U^0_{i,j} := f_{i,j}$ where f corresponds to a given color image. This implicitly defines underlying color-valued PDEs.

Obviously, in order to give a meaning to the formulae (10)–(22) in the latter setting, we must define suitable notions for maximum and minimum of up to three matrices, and we must give useful expressions for the square root and the absolute value of occuring matrices. This will be done in Section 5.

4 Color Images and Matrix Fields

In this section, we briefly recall the conversion of *rgb* values to matrices as in [11]. Given an *rgb* image we transform it in two steps into a matrix field of equal dimensions, i.e. we assign each pixel of the image a symmetric 2×2 matrix.

In the first step, we transform the *rgb* color values to the *hcl* color space, assuming that red, green and blue intensities are normalized to $[0, 1]$. For a pixel with such intensities r, g, b, we obtain its hue h, chroma c and luminance l via $M = \max\{r, g, b\}$, $m = \min\{r, g, b\}$, $c = M - m$, $l = \frac{1}{2}(M + m)$, and $h = \frac{1}{6}(g-b)/M$ modulo 1 if $M = r$, $h = \frac{1}{6}(b-r)/M + \frac{1}{3}$ if $M = g$, $h = \frac{1}{6}(r-g)/M + \frac{2}{3}$ if $M = b$, cf. [1].

Replacing then luminance l with $\tilde{l} := 2l - 1$, and interpreting c, $2\pi h$, and $\tilde{l}$ as radial, angular and axial coordinates of a cylindrical coordinate system, we have a bijection from the unit cube of triples (r, g, b) onto a solid bi-cone, see Figure 1.

The bi-cone is then transformed to the Cartesian coordinates via $x = c\cos(2\pi h)$, $y = c\sin(2\pi h)$, $z = \tilde{l}$. The second step takes the coordinates (x, y, z) and maps them to symmetric matrices $A \in \mathrm{Sym}(2)$ via

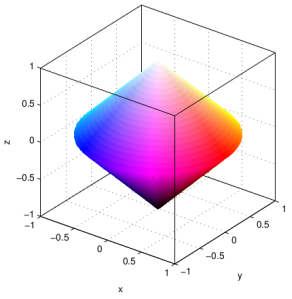

Fig. 1. Color bi-cone, figure adapted from [11]

$$A := \frac{\sqrt{2}}{2}\begin{pmatrix} z-y & x \\ x & z+y \end{pmatrix} \tag{23}$$

Note that the mapping $\Psi : \mathbb{R}^3 \to \mathrm{Sym}(2)$ in (23) is bijective.

Denoting by $\mathcal{M} \subset \mathrm{Sym}(2)$ the set of all matrices A that correspond to points of the bi-cone, we have in fact by (23) a bijection between the *rgb* color space and the bi-cone $\mathcal{M}$. The inverse transform is obtained in a straightforward way, cf. [11].

5 Pseudo Supremum and Infimum and Functions of Matrices

As indicated at the end of Section 3, we need to give meaning to the maximum and minimum of up to three matrices of Sym(2), as well as to the square root and the absolute value of such matrices. Thereby we rely on corresponding notions as discussed e.g. in [7].

Let us recall that any matrix $A \in \mathrm{Sym}(2)$ can be decomposed into the format $A = V\,\mathrm{diag}(\lambda_1, \lambda_2)V^\top$ where $V := (v_1, v_2)$ accumulates the eigenvectors v_1, v_2 of A as column vectors and $\lambda_{1,2}$ denote the corresponding eigenvalues. Then one may define a function φ of a matrix A via

$$\varphi(A) := V\,\mathrm{diag}(\varphi(\lambda_1), \varphi(\lambda_2))V^\top \tag{24}$$

in terms of its standard scalar representation. With $\varphi(\cdot) = \sqrt{\cdot}$ and $\varphi(\cdot) = |\cdot|$ we thus obtain square root and absolute value of a symmetric matrix, respectively.

Regarding the formulae of numerical schemes in Section 3, we need to calculate the maximum and minimum of up to three symmetric matrices. It will turn out that instead of maximum and minimum we will seek a supremum and infimum, respectively, and it will suffice to elaborate in detail on the supremum.

Let us consider matrices $A, B, C \in \mathrm{Sym}(2)$. Determining the supremum of two such matrices can be done making use of (24) by

$$\sup(A, B) \;:=\; \frac{A+B}{2} + \frac{|A-B|}{2} \tag{25}$$

adopting a corresponding scalar relation. Obviously, we can proceed by

$$\begin{aligned} \sup_1 &:= \sup(A, \sup(B, C))\,, \\ \sup_2 &:= \sup(B, \sup(A, C))\,, \\ \sup_3 &:= \sup(C, \sup(A, B)) \end{aligned} \tag{26}$$

But generally, for $A, B, C \in \mathrm{Sym}(2)$ we have

$$\sup_1 \;\neq\; \sup_2 \;\neq\; \sup_3 \;\neq\; \sup_1 \tag{27}$$

Consequently, we approximate the supremum of $\{A, B, C\}$ by calculating the average of $\sup_1$, $\sup_2$ and $\sup_3$, as the $\sup_{avg}$ which is an upper bound of each initial matrix.

To improve this often very generous upper bound, we find the optimal value of $\eta \geq 0$ in such a way that

$$\sup_{avg} - \eta I \;\geq\; W\,, \qquad W \in \{A, B, C\}\,, \tag{28}$$

where I is the 2×2 identity matrix. The optimal amount η_{opt} of η in (28) is the minimum eigenvalue of $(\sup_{avg} - A)$, $(\sup_{avg} - B)$, and $(\sup_{avg} - C)$. At the end of this process, we obtain a proper supremum of $\{A, B, C\}$ as

$$\sup_{opt}(A, B, C) \;:=\; \sup_{avg} - \eta_{opt} I \tag{29}$$

To obtain an infimum of three matrices, one may simply set

$$\inf_{opt}(A, B, C) \;:=\; \sup_{opt}(-A, -B, -C) \tag{30}$$

6 Experiments

As the first experiment we test if our color morphology operations retrieve gray-scale morphology, since this may be considered a necessary condition to obtain a reasonable extension of the latter. To this end, we employ *rgb* values for black and white and use the new color-valued FCT scheme as described in Section 3. In Fig. 2 we exhibit the result of dilation and erosion on the *yin-yang* image of size 256×256.

Fig. 2. Centre. Input image yin-yang defined using *rgb* values for black and white. **Left.** Ten times dilation with color-valued FCT. **Right.** Ten times erosion with color-valued FCT.

Operations are performed ten times with time step size $\tau = 1/2$ and the disk-shaped stucturing element. As observed, outcomes are equivalent to gray-scale morphology.

In our second test we aim to observe dilation and erosion in color space with the RT scheme. The reasoning is here, that independently from its usefulness by its own the RT scheme serves as the basis of the FCT method and it is very similar to the first-order method that the OS scheme builds upon. Therefore, it is of fundamental importance for our PDE-based approach that the RT scheme yields reasonable results, as otherwise the more advanced OS and FCT schemes cannot be expected to do something valuable.

As observed in Fig. 3 we can confirm that the RT scheme performs as expected. Taking the classic *Lena* test image of resolution 128×128 as input image, we see that after six iterations of dilation and erosion with time step size $\tau = 1/2$ that bright and dark colors are enhanced, respectively. The blurring we observe here is the standard numerical artefacts resulting from the first-order upwind discretization. In an extension of these experiments, we compute the morphological Laplacian and show results of shock filtering based on our framework using also the RT scheme with $\tau = 1/2$. As observed, we obtain visually very plausible results for this process. Let us note that for the purpose of shock filtering the RT scheme is the optimal PDE-based method since the shock-filtering process is designed to give sharp edges.

Our next experiment serves two purposes. On the one hand we compare the quality of the numerical schemes RT, OS, and FCT in our new framework in order to see if the non-linear operations performed in the algorithms still give reasonable, interpretable results. On the other hand, we compare here with the method of Burgeth and Kleefeld (BK) [11] that is technically more similar to classic, lattice-based morphology than our PDE-based schemes. Let us emphasize in the latter context again, that the BK method employs the same color space yet with a different means of addition and subtraction of color matrices. Let us note that we employ in BK a cross-shaped structuring element here as the approximation of a disk on a 3×3 grid.

To this end, we employ a test image based on a micro biological scene, based on an oil painting of Carolyn K. Snyder. It is of resolution 128×128 and features diverse colors as well as round structures, see Fig. 4.

Fig. 3. Top row. Original *Lena* image, and results of dilation and erosion computed with the RT scheme. **Bottom row.** Morphological Laplacian and results of five and ten iterations of shock filtering with the RT scheme.

The results of our comparison are displayed in Fig. 5 where we show the images after several dilation steps. They show that all of the PDE-based methods give results of expected quality. The RT scheme yields a blurry dilated image and the FCT scheme very sharp edges while the OS method is somewhere in between those schemes. We also see no obvious color distortions, and round shapes evolve in a round way as by the underlying disk-shaped structuring element used for the PDE-based methods. In the result of the BK method for discrete morphology, we recognize the influence of the cross-shaped structuring element while we do not observe other color effects as in the results of the PDE-based schemes, although these employ different addition and subtraction rules. Note that the PDE-based FCT method gives visually as sharp edges as the BK method.

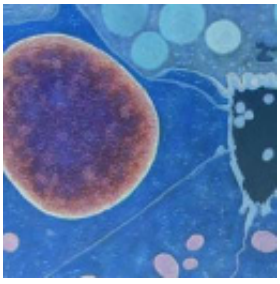

Fig. 4. Input image for comparison of numerical methods

Our next and final experiment is dealing with the influence of the color space. Obviously, the value of the pseudo supremum resp. infimum of two colors in the dilation resp. erosion process is dependent on the location of those colors in the bi-conal color structure. Generally, the pseudo supremum of any color faced with

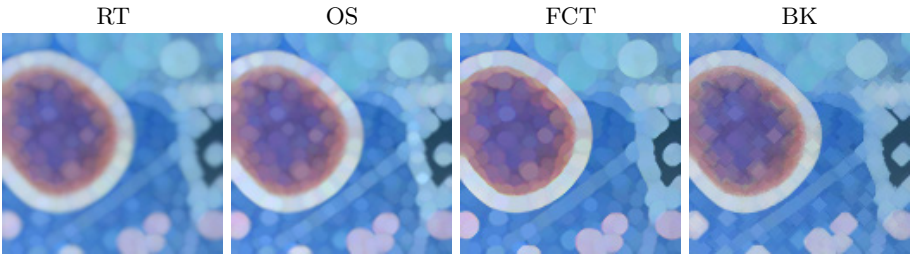

Fig. 5. Results of eight time steps dilation with $\tau = 1/2$ for indicated PDE-based schemes and in accordance four times erosion of BK method.

white is white and the pseudo infimum of any color faced with black is black. Thus we will not see any new appearing color at the edge to a black or white region.

Also in other cases, if one of the primary colors equals the pseudo supremum or infimum of them, then we do not have any color changes in the border of those colors during basic morphological operations. Some examples of this situation are indicated in Fig. 6 by yellow frames. But, if the pseudo supremum or infimum of the two colors equals another color, it appears as a modified color. Some situations like these are marked with black frames in Fig. 6. Note that the new colors are not false colors [23] but appear as more resp. less saturated versions of bordering colors.

Let us investigate this phenomenon at hand of an example dealing with the colors *light magenta (lm)*, *dark magenta (dm)* and *cyan (cy)*. Light magenta has the *rgb* values $(252, 58, 157)$, the numbers are $(217, 57, 153)$ for dark magenta,

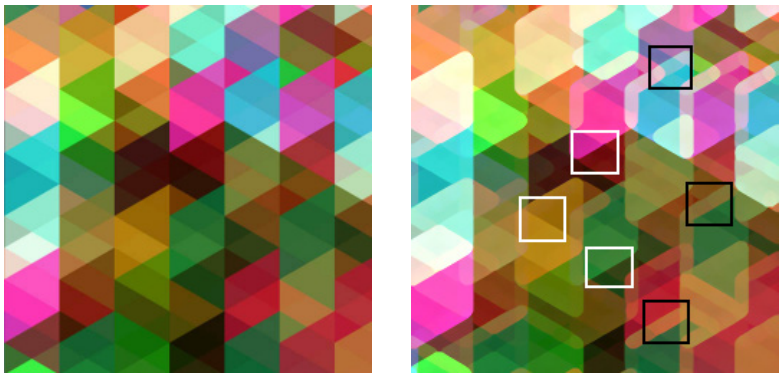

Fig. 6. Original image of size 256×256 (left) and result after five iterations of dilation using FCT with $\tau = 1/2$ and a disk-shaped structuring element. Black frames indicate new colors that appear by use of the supremum rule and the yellow ones mark color interaction without new colors.

and $(62, 186, 212)$ for cyan. The equivalent matrices of these colors are as follows (entries rounded):

$$\text{lm} = \begin{bmatrix} 0.427 & 0.463 \\ 0.463 & -0.122 \end{bmatrix}, \quad \text{dm} = \begin{bmatrix} 0.314 & 0.359 \\ 0.359 & -0.208 \end{bmatrix}, \quad \text{cy} = \begin{bmatrix} 0.128 & -0.409 \\ -0.409 & -0.022 \end{bmatrix} \tag{31}$$

By computing corresponding pseudo suprema of two matrices, we obtain (rounded):

$$\sup(\text{lm},\text{dm}) = \begin{bmatrix} 0.429 & 0.461 \\ 0.461 & -0.119 \end{bmatrix}, \quad \sup(\text{dm},\text{cy}) = \begin{bmatrix} 0.616 & -0.025 \\ -0.025 & 0.280 \end{bmatrix} \tag{32}$$

The *rgb* amounts of the first pseudo supremum are $(252, 59, 157)$, while in the second one we gain $(200, 178, 239)$.

These observations show that during a dilation process, for the left inner edge as seen in Fig. 7, we have a color almost like light magenta which appears at the border as the extension of the light magenta color, while in the right inner border, a new color emerges as the supremum of the dark magenta and the cyan areas. However, observe also here that this is not a false color.

Fig. 7. Colors in the example

7 Conclusion

In this paper, we have proposed a new approach for implementing various morphological operators for color images using PDE-based methods. The numerical experiments done with Matlab show that we obtain qualitatively competitive results to a recent approach from the literature [11], while our approach offers the conceptual benefits of digital scalability and potential sub-pixel accuracy.

References

1. Agoston, M.K.: Computer Graphics and Geometric Modeling: Implementation and Algorithms. Springer, London (2005)
2. Alvarez, L., Guichard, F., Lions, P.-L., Morel, J.-M.: Axioms and fundamental equations in image processing. Archive for Rational Mechanics and Analysis **123**, 199–257 (1993)
3. Aptoula, E., Lefèvre, S.: A Comparative Study on Multivariate Mathematical Morphology. Pattern Recognition **40**(11), 2914–2929 (2007)
4. Arehart, A.B., Vincent, L., Kimia, B.B.: Mathematical morphology: The Hamilton-Jacobi connection. In: Proc. Fourth International Conference on Computer Vision pp. 215–219 (1993)
5. Breuß, M., Weickert, J.: A Shock-Capturing Algorithm for the Differential Equations of Dilation and Erosion. Journal of Mathematical Imaging and Vision **25**(2), 187–201 (2006)

6. Brockett, R.W., Maragos, P.: Evolution equations for continuous-scale morphology, In: Proc. IEEE International Conference on Acoustics, Speech and Signal Processing vol. 3, 125–128 (1992)
7. Burgeth, B., Breuß, M., Didas, S., Weickert, J.: PDE-based Morphology for Matrix Fields: Numerical Solution Schemes, Tensors in Image Processing and Computer Vision, pp. 125–150 (2009)
8. Burgeth, B., Bruhn, A., Didas, S., Weickert, J., Welk, M.: Morphology for tensor data: ordering versus PDE-based approach. Image and Vision Computing **25**(4), 496–511 (2007)
9. Burgeth, B., Kleefeld, A.: An approach to color-morphology based on Einstein addition and Loewner order. Pattern Recognition Letters **47**, 29–39 (2014)
10. Comer, M.L., Delp, E.J.: Morphological operations for color image processing. J. Electron. Imaging **8**(3), 279–289 (1999)
11. Goutsias, J., Heijmans, H.J.A.M., Sivakumar, K.: Morphological operators for image sequences. Computer Vision and Image Understanding **62**, 326–346 (1995)
12. van de Gronde, Jasper J., Roerdink, Jos B.T.M.: Group-invariant frames for colour morphology. In: Hendriks, Cris LLuengo, Borgefors, Gunilla, Strand, Robin (eds.) ISMM 2013. LNCS, vol. 7883, pp. 267–278. Springer, Heidelberg (2013)
13. Haralick, R.M., Sternberg, S.R., Zhuang, X.: Image analysis using mathematical morphology. IEEE Trans. Pattern Anal, Machine Intell **9**(4), 532–550 (1987)
14. Matheron, G.: Eléments Pour une Thorie des Milieux Poreux. Masson, Paris (1967)
15. Osher, S., Rudin, L.I.: Feature-oriented image enhancement using shock filters. SIAM Journal on Numerical Analysis **27**, 919–940 (1990)
16. Osher, S., Sethian, J.A.: Fronts propagating with curvature-dependent speed: algorithms based on Hamilton-Jacobi formulations. J. of Computational Physics **79**, 12–49 (1988)
17. Rouy, E., Tourin, A.: A viscosity solutions approach to shape-from-shading. SIAM Journal on Numerical Analysis **29**, 867–884 (1992)
18. G. Sapiro, Geometric Partial Differential Equations and Image Analysis, pp. 96–102. Cambridge University Press (2001)
19. Sapiro, G., Kimmel, R., Shaked, D., Kimia, B.B., Bruckstein, A.M.: Implementing continuous-scale morphology via curve evolution. Pattern Recognition **26**, 1363–1372 (1993)
20. Serra, J.: Échantillonnage et estimation des phénomènes de transition minier, Ph.D thesis, University of Nancy, France (1967)
21. Serra, Jean: The "False Colour" problem. In: Wilkinson, Michael H.F., Roerdink, Jos B.T.M. (eds.) ISMM 2009. LNCS, vol. 5720, pp. 13–23. Springer, Heidelberg (2009)
22. van den Boomgaard, R.: Mathematical Morphology: Extensions Towards Computer Vision, Ph.D thesis, University of Amsterdam, The Netherlands (1992)
23. van Vliet, L.J., Young, I.T., Beckers, A.L.D.: A nonlinear Laplace operator as edge detector in noisy images. Computer Vision, Graphics and Image Processing **45**(2), 167–195 (1989)